Available online at www.sciencedirect.com
SCIENCE DIRECT
Journal of Power Sources 146 (2005) 134–141
JOURNAL OF POWER SOURCES
www.elsevier.com/locate/jpowsour

Behaviour of highly crystalline graphites in lithium-ion cells with propylene carbonate containing electrolytes

H. Buqa [a,*], A. Würsig [a], D. Goers [a], L.J. Hardwick [a], M. Holzapfel [a], P. Novák [a], F. Krumeich [b], M.E. Spahr [c]

[a] *Paul Scherrer Institut, Electrochemistry Laboratory, CH-5232 Villigen PSI, Switzerland*
[b] *Swiss Federal Institute of Technology, Laboratory of Inorganic Chemistry, CH-8093 Zürich, Switzerland*
[c] *TIMCAL Ltd., CH-6743 Bodio TI, Switzerland*

Available online 25 April 2005

Abstract

Several TIMREX® synthetic and natural graphite negative electrode materials with different particle size distributions were tested with regard to their compatibility with propylene carbonate used as electrolyte component in lithium-ion cells. The first lithium insertion properties of these graphite materials were characterised in electrochemical lithium half-cells containing 1 M $LiPF_6$ in ethylene carbonate/propylene carbonate as electrolyte system. *Post mortem* scanning electron microscopy was applied to study the exfoliation process observed for some of these graphite materials especially with coarser particle sizes. X-ray diffraction, Raman spectroscopy and nitrogen gas adsorption were used to characterise and correlate the material bulk and surface properties of the graphite materials with their electrochemical performance. Differential electrochemical mass spectrometry was applied to study the passivation process of the graphite material surface during the first electrochemical reduction. Non-exfoliating graphite materials indicate the formation of an efficient solid electrolyte interphase, which seems to be kinetically controlled by intrinsic properties of the graphite material bulk and surface.

Keywords: Propylene carbonate electrolyte; Graphite exfoliation; Graphite negative electrode materials; Rechargeable lithium batteries

1. Introduction

Graphitic carbon materials are the current materials of choice for the negative electrode in commercial lithium-ion batteries. Among these graphitic carbons, the highly graphitised materials are particularly attractive due to their high reversible specific charge of up to 372 mAh g^{-1}, good cycling stability as well as a high electronic conductivity. The formation of an efficient passivation film on the graphite particle surface during the first electrochemical reduction is essential for the proper functioning of these electrode materials in the lithium-ion battery. This passivation film, the solid electrolyte interphase (SEI), is the key component for the achievement of good reversibility of the electrochemical insertion process, as well as a high energy density and high rate performance [1,2]. The nature of the electrolyte strongly influences the performance of the graphite negative electrode. In particular, not all electrolyte systems are compatible with graphitic carbon-based electrodes. Ethylene carbonate (EC) is known as a good film-forming solvent component in the battery electrolyte [3–5], while propylene carbonate (PC) containing electrolytes are reported to show a rather poor behaviour, especially with synthetic graphite materials [6,7]. Unfortunately, EC cannot be used as single solvent for room temperature applications due to its high melting point, a low viscosity causing low electrolyte conductivities as well as a poor wettability. It has to be mixed with co-solvents to sufficiently enhance its low-temperature performance. Mixtures of EC with dimethyl carbonate (DMC) or diethyl carbonate (DEC) are usually chosen as electrolyte for lithium-ion cells [2,6]. However, PC-based electrolytes are more favourable with respect to their superior low temperature behaviour [4,6,8,9], flash point and stability against oxidation. But, the use of

* Corresponding author.
E-mail address: hilmi.buqa@psi.ch (H. Buqa).

0378-7753/$ – see front matter © 2005 Elsevier B.V. All rights reserved.
doi:10.1016/j.jpowsour.2005.03.106

PC is limited if graphite negative electrode materials with a high degree of graphitisation are used. This limitation is ascribed by Besenhard et al. to a phenomenon called solvent co-intercalation, causing graphite exfoliation, i.e., destruction of the crystal lattice [3,8]. Particularly in the first charge cycle, before the formation of the protective SEI film on Li_xC_6 is finished, the tendency for solvent co-intercalation is high [9]. The exfoliation is finally stopped by the formation of a protecting SEI film. Aurbach et al. [10,11] suggested that in PC solutions graphite particles crack due to gas formation on the graphite surface and within existing surface cavities. The graphite anodes are thus "deactivated" due to electrical isolation of the cracked particles by surface films.

The influence of the electrolyte system on the exfoliation process has been studied in several publications, but still little is known about the influence of the particular solvent components on the solvent co-intercalation process, which seems to be responsible for the graphite exfoliation process that can be observed in the case of some graphite materials [12–15]. Besides the electrolyte system, the graphite material properties also influence the graphite passivation process. The critical material parameters reported are the surface chemistry and morphology, the ratio of basal planes to edge planes, particle size distribution, the ratio of rhombohedral and hexagonal phase in the graphite crystal structure and the existence of a certain disorder on the particle surface [14,16,17]. Careful investigation of all the factors which play a crucial role for the graphite passivation or graphite exfoliation, as well as their interaction should give a clearer picture of the complexity of the SEI layer composition and the SEI formation mechanism.

In this paper, a systematic study of the first electrochemical intercalation of lithium into several synthetic and natural graphites in EC/DMC and EC/PC mixtures containing 1 M $LiPF_6$ is presented. The passivation process of these graphite materials is compared by several in situ and ex situ methods and correlated with the graphite material bulk and surface properties.

2. Experimental

Different types of TIMREX® (TIMCAL SA, Bodio, Switzerland) graphite materials were used as negative electrode materials. Synthetic (SFG, KS) as well as natural (E-LSG) graphite material were applied as received [18]. The samples have particle sizes (d_{90}) varying from 4 to 75 μm. The number in the graphite designation indicates the d_{90} particle size value. For example, in samples with the number 6 (SFG6, KS6 and E-LSG6) 90% of the particles are smaller than 6 μm. The basic parameters of all samples are summarised in Table 1. For the determination of the specific BET surface area, nitrogen gas adsorption measurements were performed at 77 K using a Micromeritics ASAP2010. The particle size distribution was determined by laser diffraction (MALVERN Mastersizer).

The crystallinity of the graphite materials was characterised by X-ray diffraction (XRD) measurements with a STOE Stadip diffractometer in Debye–Scherrer geometry using monochromatic Cu $K\alpha_1$ radiation (1.5418 Å). The average crystallite size along the crystallographic *c*-axis (L_c) and the *a*-axis directions (L_a) were determined from the FWHM of the carbon (0 0 2) and (1 0 0) Bragg reflexes, respectively, after correction by the factor for the instrumental broadening [19]. The rhombohedral fraction (3R phase) was derived by the comparison of the intensities of the (1 0 1) hexagonal and rhombohedral diffraction peaks.

Table 1
Structural bulk parameters, surface properties and results of the electrochemical charge/discharge measurements (1st cycle irreversible charge losses) of different TIMREX® graphites in 1 M $LiPF_6$, EC/DMC and EC/PC electrolyte

Graphite	BET ($m^2\,g^{-1}$)	d_{50}[a] (μm)	Rhombohedral 3R-phase[b] (%)	L_c (Å) [XRD]	L_a (Å) [XRD]	L_a (Å)[Raman]	Irreversible charge loss [1st cycle] (%)	
							EC/DMC	EC/PC
SFG6	17.1	3.3	37	303	622	240	20	19
SFG10	10.4	6.7	29	360	565	630	17	57
SFG15	8.8	9.1	23	365	609	760	12	62
SFG44	4.6	23.9	17	401	572	530	7.2	87
SFG75	3.3	29.0	16	399	597	680	6.5	89
KS4	19.4	3.6	40	205	345	200	30	34
KS6	13.8	5.6	29	275	475	210	24	65.2
KS10	12.3	7.5	19	305	613	620	21.5	80.5
KS15	12.0	8.2	25	297	520	460	20	82
KS44	6.2	20.0	12	313	557	390	13	88.5
KS75	3.0	24.0	11	336	543	450	11	91
E-LSG6	14.2	3.5	41	335	507	340	18	19
E-LSG15	8.5	8.9	29	353	566	620	14.2	14
E-LSG44	4.5	22.9	21	405	600	420	8.4	81

Structural bulk parameters of graphite were obtained from X-ray diffraction measurements. The particle size distribution of the graphite was determined by laser diffraction (MALVERN Mastersizer). Surface properties: listed specific BET surface areas were obtained from nitrogen adsorption measurements, and Raman spectroscopy was used to characterise the crystallinity in the surface-near regions of the graphite particles (L_a-values).

[a] For example, in sample SFG6, 50% of the particles are smaller than 3.3 μm.

[b] Fraction of the rhombohedral phase (3R) in graphite.

Raman spectroscopy was used to determine the graphite crystallite length along the *a*-axis (L_a) of the near-surface layers of graphite samples. A confocal Raman microscope (Labram series, Jobin Yvon SA, ex DILOR SA) acquired the Raman spectra. A HeNe Laser (632.8 nm) illuminated the sample with ca. 2.5 mW of laser power. Raman spectra were recorded in the spectral range of 1000–1900 cm^{-1}, under confocal conditions, employing an $\times 100$ objective, with a spatial resolution of 1–2 μm^3. The L_a-value was calculated from the D- and G-band ratio using the equation proposed by Tuinstra and Koenig [20]. The full calculation method has been explained elsewhere [21,22]. The graphite samples were measured as received and the average L_a-values were derived from Raman maps created from 225 spectra recorded from squares of 40 $\mu m \times 40$ μm located on several randomly selected points on the graphite surface. For each map the band intensity ratio was calculated using the Dilor Software Package and Microcal Origin was employed to derive the mean L_a-value.

The electrochemical measurements were performed at 25 °C in a gas-tight coin-cell-like arrangement [23]. Electrodes were prepared by blade-coating the graphite on a copper foil. Ten weight percent of polyvinylidene difluoride (Solef 1015) was used as binder. The geometric electrode area was 1.33 cm^2. Metallic lithium was used as the reference and counter electrodes.

Unless otherwise stated, galvanostatic measurements were performed at a low current density of 10 mA g^{-1} of carbon to allow for the complete formation of the SEI. After a potential of 5 mV versus Li/Li^+ was reached, the charging continued potentiostatically until the specific current dropped below 5 mA g^{-1}. The electrochemical lithium de-insertion was performed at a constant current of 10 mA g^{-1} until a cut-off potential of 1.5 V versus Li/Li^+ with subsequent potentiostatic stabilisation at this potential until the specific current dropped below 5 mA g^{-1}.

The electrodes for the post mortem scanning electron microscopy (SEM) studies were first galvanostatically charged at 10 mA g^{-1} to 300 mV versus Li/Li^+, then the cells were equilibrated at 298 K for 48 h at this potential. Afterwards, the cells were dismantled, the graphite electrodes washed with dry DMC, and dried in an argon atmosphere. SEM studies were performed on a LEO 1530 Gemini microscope, which was operated at low voltage (usually 1 kV) to achieve a suitable contrast of the surface details in the secondary electron images and to minimise charging of the uncoated samples.

Differential electrochemical mass spectrometry (DEMS) was used to study the processes of electrolyte decomposition and SEI formation. The formation of ethylene, propylene, hydrogen and/or carbon dioxide, respectively, on the graphite electrodes was followed during the first electrochemical reduction in the different carbonate-based electrolyte solutions. The DEMS set-up has been described elsewhere [24].

3. Results and discussion

Both, the synthetic SFG and KS as well as the natural based E-LSG graphite materials selected for this study belong to the family of highly crystalline graphite materials but show complementary properties in terms of their morphology. All KS graphite materials consist of relatively isometric particles showing comparatively isotropic properties. The SFG and E-LSG graphite materials have particles with a relatively flaky morphology and a high degree of anisotropy. Table 1 summarises the results of the detailed material characterisation analysis performed with these graphites. These materials were galvanostatically charged and discharged in lithium half-cells using 1 M $LiPF_6$ in EC/DMC 1/1 (w/w) and EC/PC 1/1 (w/w) as electrolyte system. For a detailed investigation of the film formation in the first cycle, we analyzed the irreversible charge losses and galvanostatic charge curves of the first charge/discharge cycle. Table 1 shows the electrochemical results for all graphite materials investigated. In the case of the EC/DMC electrolyte system, a reversible capacity of up to 372 mAh g^{-1}, which corresponds to a chemical composition of LiC_6 for the fully inserted graphite electrode, was measured for all graphite materials indicating the high crystalline character of the graphite materials. In fact, the difference of the graphite materials, besides the particle size distribution, lies only in the size of the single crystal domains indicated by the L_c- and L_a-values, but not in the degree of crystallinity of these crystals. The irreversible capacity increases with the BET surface area of the graphite materials, which is in agreement with other results reported for such type of carbons in the literature [25,26].

In the case of the 1 M $LiPF_6$, EC/PC 1/1 electrolyte, the first galvanostatic charge/discharge shows a strong increase of the irreversible capacity especially for the coarse graphite materials. At the same time, the reversible capacity drops significantly. The increase of the irreversible capacity is due to an additional irreversible process, which is indicated in the galvanostatic potential curves as an additional potential plateau. Depending on the type and particle size distribution of the graphite negative electrode material, this additional irreversible potential plateau during the first electrochemical lithium intercalation is observed at different potentials. During this irreversible process, the exfoliation of the graphite electrode occurs. The potential plateau corresponds to the irreversible, charge consuming process of film formation on the graphite surface freshly created by the exfoliation process. As shown in more detail in the following, the potential difference of this plateau for the different graphite materials can be correlated with the crystallinity, morphology and surface chemistry of the graphite.

Fig. 1 shows the first galvanostatic lithium insertion/de-insertion into SFG graphite with different particle sizes using 1 M $LiPF_6$ in EC/PC. With increasing particle size, the PC sensitivity of these graphite materials increases, i.e., the size of the potential plateau increases. (Note that the large "*x*"

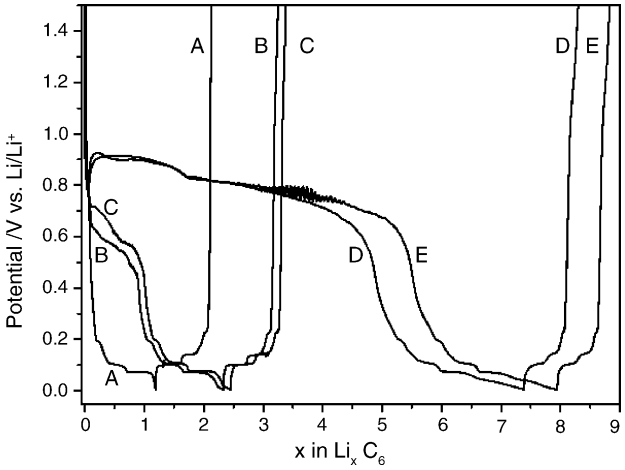

Fig. 1. First electrochemical intercalation/de-intercalation cycle of lithium into TIMREX® SFG graphite with different average particle size in 1 M $LiPF_6$, EC/PC (1/1) as electrolyte: (A) SFG6, (B) SFG10, (C) SFG15, (D) SFG44 and (E) SFG75.

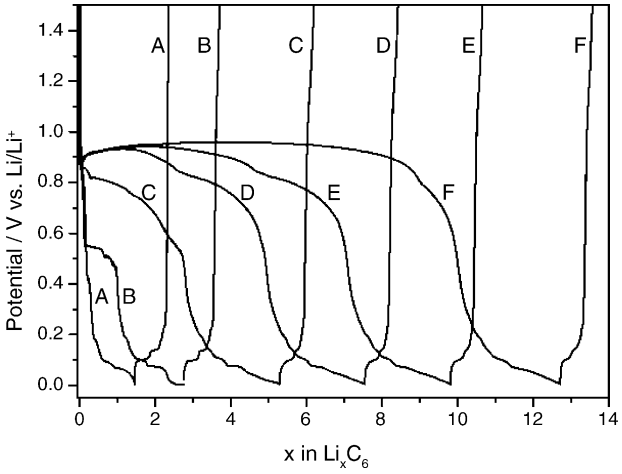

Fig. 2. First electrochemical intercalation/de-intercalation cycle of lithium into TIMREX® KS graphite with different average particle size in 1 M $LiPF_6$ in EC/PC (1/1) electrolyte: (A) KS4, (B) KS6, (C) KS10, (D) KS15, (E) KS44 and (F) KS75.

values in Fig. 1 are fictitious because of the exfoliation, i.e., there is no real compound Li_6C_6 or Li_8C_6.) Whereas in case of SFG6 (graphite A in Fig. 1) with $d_{50\%} = 3.3\,\mu m$ no additional irreversible potential plateau can be observed, SFG44 (graphite D) with a $d_{50\%}$ of 23.9 μm indicates a strong irreversible process. At the same time, the initial potential of the start of the irreversible process shifts to more positive potentials, the coarser the SFG graphite materials are. For the SFG6 material, the short plateau at ca. 800 mV versus Li/Li^+ corresponds to the SEI film formation. In the case of SFG10 (graphite B, $d_{50\%} = 6.7\,\mu m$), an additional plateau appears starting at a potential of about 0.65 V versus Li/Li^+. This irreversible plateau corresponds to graphite exfoliation. The same type of plateau is observed at about 0.72 V versus Li/Li^+ for SFG15 (graphite C, $d_{50\%} = 9.1\,\mu m$). Interestingly, in the case of SFG 44 (graphite D, $d_{50\%} = 23.9\,\mu m$) and SFG75 (graphite E, $d_{50\%} = 29\,\mu m$) the initial potential of the irreversible process is at about 900 mV versus Li/Li^+ and seems to be independent of the particle size distribution. The potential differences of the irreversible plateaus indicate different reduction mechanisms of the EC/PC electrolyte.

Almost the same trend as for the SFG graphites was observed for the KS graphites, as shown in Fig. 2. The discharge curve for the KS4 graphite (graphite A in Fig. 2 with a particle size of about 3.6 μm) shows the SEI formation plateau around 0.80 V versus Li/Li^+. A small additional plateau at ca. 0.40 V versus Li/Li^+ eventually may be linked to exfoliation of a very small number of particles. Post-mortem SEM studies of the discharged KS4 electrode indicate a uniform SEI film on the surface of the KS4 electrode as presented in Fig. 4 (top). No exfoliation of the particles could be found in the SEM study.

KS6 (graphite B) displays an additional potential plateau at about 0.55 V versus Li/Li^+ during the first electrochemical lithium insertion in EC/PC (Fig. 2). This relatively low potential is not typical for the exfoliation created by the co-solvated intercalation of propylene carbonate in the graphite structure but recently was observed in case of exfoliation in an EC electrolyte [22]. The low potential of the exfoliation in propylene carbonate observed for KS6 indicates a particular electrochemical reduction mechanism of the KS6 electrode. Interestingly, the irreversible processes for all other KS graphite materials start at the same potential of about 0.90 V versus Li/Li^+. The size of the additional potential plateau increases with the particle size from KS10 (graphite C, $d_{50\%} = 7.5\,\mu m$) and KS15 (graphite D, $d_{50\%} = 8.2\,\mu m$) to KS44 (graphite E, $d_{50\%} = 20.0\,\mu m$) and KS75 (graphite F, $d_{50\%} = 24\,\mu m$). These electrochemical processes also correspond to graphite exfoliation.

Fig. 3 shows the first charge/discharge cycle of E-LSG electrodes with different particle sizes in EC/PC electrolyte. The behaviour of the E-LSG graphite materials in the mixed EC/PC electrolyte is quite similar to the behaviour of the other

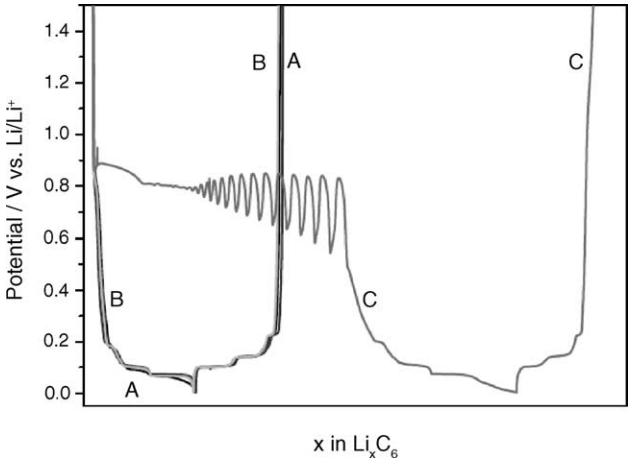

Fig. 3. First electrochemical intercalation/de-intercalation of lithium into TIMREX® E-LSG graphite with different average particle size in 1 M $LiPF_6$, EC/PC (1/1) as electrolyte: (A) E-LSG6, (B) E-LSG15 and (C) E-LSG44.

two graphite types (KS and SFG). With increasing particle size, the PC sensitivity of E-LSG increases, as was discussed for SFG graphite and KS graphites above. However, E-LSG6 (graphite A in Fig. 3) and E-LSG15 (graphite B) does not seem to exfoliate in the PC/EC electrolyte system. Both materials show similar small irreversible process at ca. 0.80 V versus Li/Li$^+$, which could correspond to the SEI film formation process.

To find an explanation for the observed differences, the graphite electrodes were charged to 300 mV versus Li/Li$^+$ and subsequently stabilised potentiostatically at this potential for 2 days. SEM images were taken from the charged graphite electrodes of the dismantled half-cells containing EC/PC electrolyte. KS4 graphite electrode (Fig. 4, top) shows a uniform and relatively dense film on the graphite particles indicating the passivation film formed by electrolyte decomposition products during the electrochemical reduction process. No exfoliation of the particles could be observed. In the case of KS75 graphite electrode (Fig. 4, bottom), exfoliation of a fraction of the graphite particles in the electrode can be observed. Some particles (mainly of larger size) show a significant expansion of their dimensions (see arrows), but other particles indicate only a partial exfoliation, i.e., the exfoliation of only some single crystals of the graphite particle. With increasing particle size, the number of exfoliated particles in the graphite electrode increases. This is manifested, at the same time, by a larger potential plateau (Fig. 2). The exfoliation of the graphite material is linked to a cleavage of some of the graphite particles until the complete destruction of the crystalline structure and amorphisation [22]. The same trend was observed for the SFG and E-LSG graphite by post mortem SEM as seen for the KS graphite (not presented in this paper).

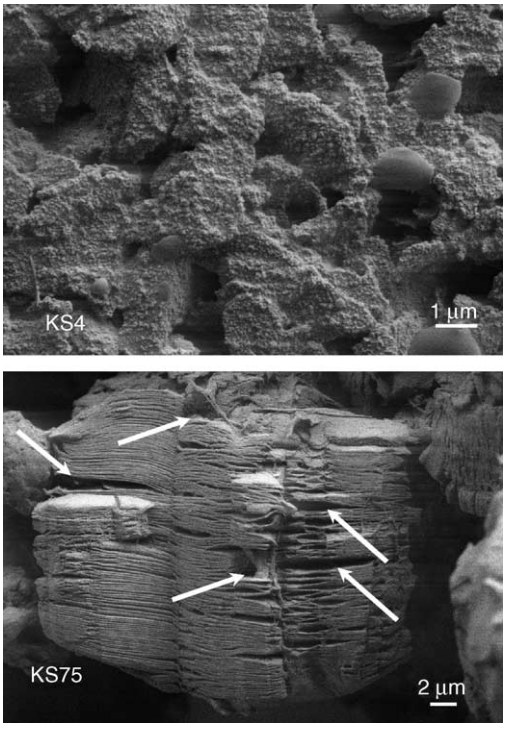

Fig. 4. Post mortem SEM images of a TIMREX® KS4 (top) and a KS75 (bottom) graphite negative electrode after stabilization at 300 mV vs. Li/Li$^+$ in a 1 M $LiPF_6$, EC/PC (1/1) electrolyte.

Comparing to the electrochemical behaviour of the SFG and KS materials in the PC/EC electrolyte, the stability of the E-LSG material in PC containing electrolytes generally seems to be higher. This could be due to a different surface morphology of the natural graphite E-LSG material. However, Raman spectroscopy measurements indicate no significantly decreased L_a-values, which could correlate with a particularly high concentration of superficial defects. High superficial defect concentration and carbon disorder has been reported as reason for the high PC stability of graphite negative electrode material [16]. Another parameter, which has been reported as responsible parameter for good stability of the graphite material in a PC containing electrolyte is the concentration of stacking defects in the graphite crystal structure [16]. In fact, the fraction of rhombohedral phase measured is higher in case of the E-LSG materials in comparison to the KS and SFG graphites with appropriate particle size distribution. Fig. 5 shows the fraction of rhombohedral fraction for different particle size distributions for the SFG, KS and E-LSG graphite powders. The rhombohedral stacking defects occurring in the bulk volume of graphite powders could be linked to a graphite surface morphology that favours a fast reaction with decomposition products resulting from the solvated EC and PC insertion process. These products precipitate on the carbon surface leading to an efficient SEI-film formation, which hinders graphite exfoliation. On the other hand, it was recently shown that even for purely hexagonal graphite the graphite exfoliation can be suppressed by optimising the surface morphology, e.g. by oxidising the graphite surface at elevated temperatures [27,30,31]. It seems quite possible, that the stability of graphites in PC containing electrolytes depends not only on one material parameter, but on a number of parameters. It might be possible that certain graphite structures, i.e., graphite materials with low amount of stacking

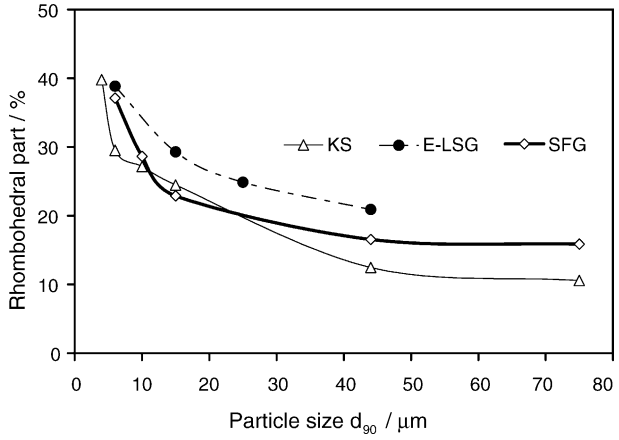

Fig. 5. Correlation between the rhombohedral fraction (XRD) and the particle size of the SFG, KS and E-LSG graphite powders.

defects have a stronger tendency to exfoliate than graphites with a higher amount of structural stacking defects. A second critical parameter, which must be considered is the graphite surface and its ability to form a passivation film during the electrochemical reduction. However, it should be noted that the rhombohedral stacking defects may only indirectly indicate the graphite stability toward PC. The graphite defect structure could be linked to a material parameter, which has not been identified yet but directly affects the exfoliation tendency [16,17].

Analyzing the data of the different graphite materials presented in Table 1 and the electrochemical behaviour in EC/PC as discussed above, it becomes evident that both, synthetic and nature graphite electrodes with a larger particle size ($d_{50} > 20$ μm) show wide additional plateaus between ca. 0.90 and 0.50 V versus Li/Li$^+$ in 1 M $LiPF_6$, EC/PC (1/1) due to the exfoliation process. An explanation could be that the exfoliation of larger particles leads to a stronger increase of the BET SSA than the exfoliation of smaller particles. Thus, the electrolyte decomposition on the larger electrode surface, which is freshly created by the exfoliation process of coarser particles, leads to a higher charge loss and a larger potential plateau. It seems also likely that electrodes consisting of larger particles are less compact and have a higher number of defects in the electrode structure and higher electrode porosity. These morphological characteristics called "free vacancies" (vacancies between neighbouring graphite particles in the electrode), can easily lead to exfoliation due the greater amount of contact area between the liquid electrolyte and the graphite surface during the reduction of solution species throughout the first cathodic polarisation [28]. The amount of such free vacancies is directly correlated with the particle shape of the graphite and thus plays an important role in the SEI film formation. We suppose that, the higher contingent of vacancies in the electrode in the case of larger particles provides a higher probability for solvent co-intercalation at the electrode surface thus favouring the electrochemical exfoliation of the graphite during the first electrochemical reduction.

Fig. 6 shows the correlation between the crystallite size in *c*-direction (L_c) and the particle size of the tested graphite materials. Generally, graphites with coarser particle size distribution show larger L_c-values and have a higher tendency towards exfoliation. However, there is no clear correlation between the L_c-values and the differences of PC compatibility between the three different graphite families.

Due to the smaller penetration depth of the Raman laser beam (some micrometers) compared to the X-ray beam, Raman spectroscopy was used to characterise the crystallinity in the surface-near regions of the graphite particles. Fig. 7 shows the L_a-values calculated from the intensity ratio of the D- and G-band observed in Raman spectroscopy. Generally, graphite materials with coarse particles show higher values for the correlation length L_a, i.e., a higher surface crystallinity and a lower concentration of superficial disordered carbon at the surface. We could say that coarse particles with larger L_a-values have a stronger tendency to exfoliate in the

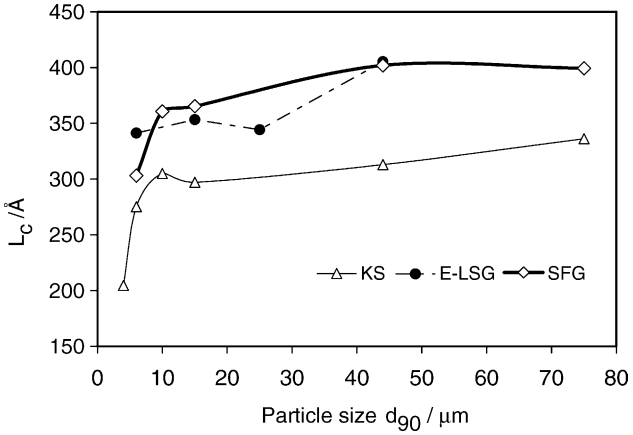

Fig. 6. Correlation between the L_c-value (XRD) and the particle size for the SFG, KS and E-LSG graphite powders.

PC/EC electrolyte within one graphite family. SFG6 has a low L_a-value of 240 Å (high amount of disorder) and does not exfoliate whilst SFG75 with a L_a-value of 680 Å (organised structure with fewer defects) exfoliates. Therefore, these results may verify that graphitic materials, which possess a more ordered structure, are more vulnerable to layer opening, which permits the intercalation of solvated lithium-ions at the beginning of the electrochemical reduction cycle [29]. However, the results of the Raman measurements do not give an explanation for the differences in PC compatibility between the different graphite families.

As already discussed above, besides the graphite crystal structure, texture and particle size distribution the graphite surface can also affect the ability to passivate during the first electrochemical reduction. A possible explanation for the difference in the SEI film formation mechanism for different materials can be deduced from differential electrochemical mass spectrometry measurements. The evolution of volatile reaction products was monitored as a function of the graphite potential for the first electrochemical insertion/de-insertion cycle of lithium into graphite using a mixed EC/PC elec-

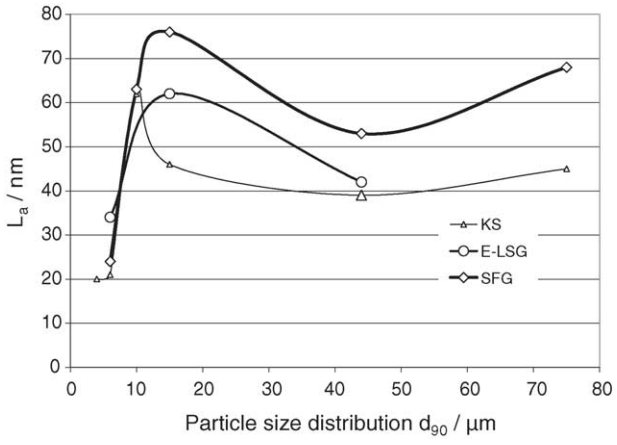

Fig. 7. Correlation between the L_a-value (Raman) and the particle size for the SFG, KS and E-LSG graphite powders.

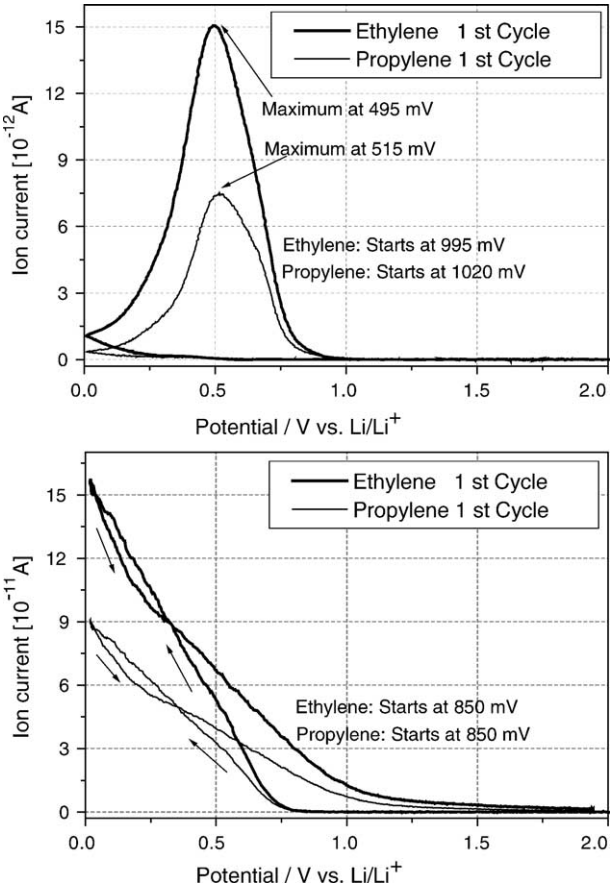

Fig. 8. DEMS measurements in half-cells with SFG6 (top) and SFG44 (bottom) vs. metallic Li and 1 M $LiPF_6$, EC/PC (1/1) electrolyte. The mass signals corresponding to ethylene ($m/z = 27$) and propylene ($m/z = 41$) formation were monitored as a function of the potential applied to the graphite electrode at a scan rate of 0.4 mV/s (MSCV mode).

trolyte system. Besides non-volatile polymeric decomposition products, which are deposited on the electrode surface, hydrogen, ethylene and propylene gas are typically formed during the electrochemical decomposition of EC/PC electrolytes [32]. The ethylene and the propylene gas formation were used to monitor the graphite passivation and film forming process. Fig. 8 shows, in the case of SFG6 and SFG44 graphite electrodes, the mass spectrometric cyclic voltamograms (MSCVs) of mass $m/z = 27$ and 41, representing the mass signal of the ethylene and propylene gas fragments, respectively. In the case of SFG6 (Fig. 8, top) the initial ethylene and propylene formation could be detected for both gases at about 1.0 V versus Li/Li^+. The ethylene and propylene signals show a maximum at 495 and 515 mV versus Li/Li^+, respectively, and almost disappears at potentials negative to 200 mV versus Li/Li^+. The electrochemical reduction of ethylene and propylene carbonate apparently is responsible for the SEI film formation process, which is completed at more positive potentials than the initial exfoliation of graphite particles. Another hint for the completed formation of the SEI film in the first cycle is the fact that almost no gas evolution can be observed during the second charge/discharge cycle.

For SFG44 the formation of both ethylene and propylene is shifted to less positive potentials and starts concurrently at ca. 0.85 V versus Li/Li^+. Obviously, the graphite passivation formation of an effective SEI film is hindered on the surface of the SFG44 particles. The exfoliation and subsequent degradation of the graphite structure is initiated before an effective SEI film is formed. The gas formation rate increases with decreasing potential. Gas formation can be observed even during the electrochemical Li^+ de-insertion process, indicating the electrolyte decomposition on the new surface created by the graphite exfoliation process. Graphite passivation apparently is never accomplished in the mixed EC/PC electrolyte. Thus, only in the case of SFG6 but not for SFG44, a complete graphite surface passivation during the first electrochemical lithium insertion from the EC/PC electrolyte occurs.

These DEMS measurements indicate significant differences between the SFG6 and SFG44 graphite surfaces to passivate during the first electrochemical reduction in the EC/PC electrolyte system. The differences of the passivation properties of the SFG6 and SFG44 surface might be due to differences in the surface morphology, indicated by Raman spectroscopy. The lower surface crystallinity, i.e., the higher concentration of superficial defects of SFG6 and disordered carbon could provide a higher amount of energetically favoured points at the graphite surface where the passivation could occur. It is probably, that not the smaller particle size but the increased graphite surface reactivity of the SFG6 graphite material, which is caused by this decreased surface crystallinity, could be the true reason for the stability of the SFG6 graphite in PC containing electrolyte systems.

4. Conclusions

The stability of highly crystalline graphite materials towards exfoliation of the graphite structure during the first electrochemical lithium insertion in mixed ethylene carbonate/propylene carbonate electrolyte systems depends on the passivation ability individual graphite surface. Graphite surfaces with a high defect concentration tend to passivate at more positive potentials. If the passivation process is completed before the electrochemical exfoliation starts, the graphite exfoliation process can be avoided.

Besides the surface parameters influencing the surface reactivity of the graphite electrode material with the electrolyte system, the graphite crystallinity and texture determines its exfoliation tendency. Apparently, graphite particles containing single crystals with low amount of defects tend to exfoliate easier than graphite powders containing a higher amount of crystal defects. To achieve graphite passivation and effective SEI formation before the graphite exfoliation process sets in, the electrolyte composition needs to be adjusted to the individual surface properties of the graphite used as negative electrode material.

Acknowledgements

The authors wish to thank the Swiss National Science Foundation, and the Swiss Federal Office of Education and Science (CAMELiA project) for financial support.

References

[1] E. Peled, in: J.P. Gabano (Ed.), Lithium Batteries, vol. 43, Academic Press, New York, 1983.
[2] M. Winter, J.O. Besenhard, M.E. Spahr, P. Novák, Adv. Mater. 10 (1979) 725–2047.
[3] J.O. Besenhard, M. Winter, J. Yang, W. Biberacher, J. Power Sources 54 (1995) 228.
[4] D. Aurbach, B. Markovsky, I. Weissman, E. Levi, Y. Ein-Eli, Electrochim. Acta 45 (1999) 167.
[5] R. Fong, U. von Sacken, J. Dahn, J. Electrochem. Soc. 137 (1990) 2009.
[6] M. Noel, R. Santhanam, J. Power Sources 72 (1998) 53.
[7] D. Bar Tow, E. Peled, L. Burstein, J. Electrochem. Soc. 146 (1999) 824.
[8] J.O. Besenhard, H.P. Fritz, J. Electrochem. Soc. 117 (1970) 222.
[9] K. Guerin, A. Février-Bouvier, S. Flandrois, M. Couzi, B. Simon, P. Biensan, J. Electrochem. Soc. 146 (2002) 3660.
[10] D. Aurbach, Y. Ein-Eli, J. Electrochem. Soc. 142 (1995) 1746.
[11] D. Aurbach, M. Moshkovich, Y. Gofer, J. Electrochem. Soc. 148 (2001) 155.
[12] M. Arakawa, J. Yamaki, J. Electroanal. Chem. 219 (1987) 273.
[13] S.K. Jeong, M. Inaba, T. Abe, Z. Ogumi, J. Electrochem. Soc. 148 (2001) 989.
[14] B. Simon, S. Flandrois, A. Février-Bouvier, P. Biensan, Mol. Cryst. Liq. Cryst. 310 (1998) 333.
[15] Y. Abe, Y. Mizutani, N. Kawabata, M. Inaba, Z. Ogumi, Synth. Meth. 125 (2002) 249.
[16] K. Guerin, A. Février-Bouvier, S. Flandrois, M. Couzi, B. Simon, P. Biensan, J. Electrochem. Soc. 146 (2002) 3660.
[17] H. Huang, W. Liu, L. Chen, E.M. Kelder, J. Schoonman, Solid State Ionics 110 (1998) 173.
[18] Product Information, TIMCAL Ltd., Bodio, Switzerland.
[19] K. Kinoshita, Electrochemical and Physicochemical Properties of Carbon, Wiley & Sons, New York, 1988.
[20] F. Tuinstra, J.L. Koenig, J. Chem. Phys. 53 (1970) 1126.
[21] D. Goers, H. Buqa, L. Hardwick, A. Würsig, P. Novák, Ionics 9 (2003) 258.
[22] M.E. Spahr, T. Palladino, H. Wilhelm, A. Würsig, D. Goers, H. Buqa, M. Holzapfel, P. Novák, J. Electrochem. Soc. 151 (2004) 1383.
[23] P. Novák, W. Scheifele, F. Joho, O. Haas, J. Electrochem. Soc. 142 (1995) 2544.
[24] R. Imhof, P. Novák, J. Electrochem. Soc. 145 (1998) 1081.
[25] M. Winter, P. Novák, A. Monnier, J. Electrochem. Soc. 145 (1998) 428.
[26] M.E. Spahr, H. Wilhelm, T. Palladino, N. Dupont-Pavlovsky, D. Goers, F. Joho, P. Novák, J. Power Sources 119–121 (2003) 543.
[27] F. Joho, B. Rykart, A. Blome, P. Novák, H. Wilhelm, M.E. Spahr, J. Power Sources 97–98 (2001) 78.
[28] H. Buqa, D. Goers, M. Holzapfel, M.E. Spahr, P. Novák, J. Electrochem. Soc. 152 (2005) A474.
[29] H. Shi, J. Baker, M. Saidi, R. Koksbang, J. Electrochem. Soc. 143 (2002) 3466.
[30] M.E. Spahr, H. Wilhelm, F. Joho, P. Novák, ITE Lett. Batteries, New Technol. Med. 2 (3) (2001) 53.
[31] M.E. Spahr, H. Wilhelm, F. Joho, J.-C. Panitz, J. Wambach, P. Novák, N. Dupont-Pavlovsky, J. Electrochem. Soc. 149 (2002) 960.
[32] D. Aurbach, K. Gamolsky, B. Markovsky, Y. Gofer, M. Schmidt, U. Heider, Electrochim. Acta 47 (2003) 1423.